HHS Public Access

Author manuscript

Nat Mater. Author manuscript; available in PMC 2020 February 19.

Published in final edited form as:

Nat Mater. 2020 January ; 19(1): 118–126. doi:10.1038/s41563-019-0462-9.

Hyaluronic acid-bilirubin nanomedicine for targeted modulation of dysregulated intestinal barrier, microbiome, and immune responses in colitis.

Yonghyun Lee[1,2,3], **Kohei Sugihara**[4], **Merritt G. Gillilland III**[4], **Sangyong Jon**[5], **Nobuhiko Kamada**[4], **James J. Moon**[1,2,3,*]

[1]Department of Pharmaceutical Sciences, University of Michigan, Ann Arbor, Michigan 48109, USA.

[2]Department of Biomedical Engineering, University of Michigan, Ann Arbor 48109 USA.

[3]Biointerfaces Institute, University of Michigan, Ann Arbor, Michigan 48109, USA.

[4]Division of Gastroenterology, Department of Internal Medicine, University of Michigan, 1150 W. Medical Center Drive, Ann Arbor, Michigan 48109, USA.

[5]KAIST Institute for the BioCentury, Department of Biological Sciences, Korea Advanced Institute of Science and Technology (KAIST), 291 Daehak-ro, Daejeon 34141, Republic of Korea.

Abstract

While conventional approaches for inflammatory bowel diseases (IBD) mainly focus on suppressing hyperactive immune responses, it remains unclear how to address disrupted intestinal barriers, dysbiosis of the gut commensal microbiota, and dysregulated mucosal immune responses in IBD. Moreover, immunosuppressive agents can cause off-target systemic side effects and complications. Here, we report the development of hyaluronic acid-bilirubin nanomedicine (HABN) that accumulates in inflamed colonic epithelium and restores the epithelium barriers in a murine model of acute colitis. Surprisingly, HABN also modulated the gut microbiota, increasing the overall richness and diversity and markedly augmenting the abundance of *Akkermansia muciniphila* and *Clostridium* XIVα, microorganisms with crucial roles in gut homeostasis. Importantly, HABN associated with pro-inflammatory macrophages, regulated innate immune responses, and exerted potent therapeutic efficacy against colitis. Our work sheds new light on the impact of nanotherapeutics on gut homeostasis, microbiome, and innate immune responses for the treatment of inflammatory diseases.

* moonjj@umich.edu.

Author Contributions

Y.L. and J.M. designed the experiments. Y.L. performed all experiments. K.S. and N.K. contributed technical expertise, including qPCR analysis, LPMC isolation, and flow cytometry analysis. Y.L. and J.M. analysed the data. M.G. aided with interpretation of data on gut microbiome analysis. S.J. contributed the initial design of bilirubin conjugates. Y.L. and J.M. wrote the paper.

Competing interests

The authors declare that they have no competing interests.

Additional Information

Supplementary information can be found at www.nature.com/. Information about reprints and permissions is available online at http://npg.nature.com/reprintsandpermissions.

Pathogenesis of IBD is associated with disrupted intestinal barrier functions[1,2], imbalance of the gut microbiome[3-5], and subsequent dysregulated mucosal immune responses to gut commensal bacteria[3-5]. Traditional medical interventions for IBD have mainly focused on managing the symptoms of IBD by suppressing immune responses[6]; however, they generally do not address the underlying causes of IBD, including damaged mucus layer in the gastrointestinal tract, subsequent loss of intestinal barrier functions, and dysbiosis of the gut commensal microorganisms. Moreover, despite advances in localized drug delivery[7-9], conventional immunosuppressive drugs based on small molecules or biologics can cause off-target systemic side effects, and their long term use may lead to serious complications, such as opportunistic infections, malignancies, autoimmunity, and liver toxicity[6,10]. Towards the goal of addressing this unmet medical need, we have developed a new nanotherapeutic platform that can target inflamed colonic epithelium, modulate the gut microbiome, and promote anti-inflammatory immune responses in local tissues, with improved efficacy compared with traditional IBD therapeutics in a murine model of acute colitis.

We have designed HABN system that is formed by nano-aggregation of an amphiphilic conjugate between hyaluronic acid and bilirubin. Hyaluronic acid (HA), which is a glycosaminoglycan biopolymer commonly found in synovial fluid and extracellular matrix, has immunomodulatory properties, including regulation of macrophages[11], induction of anti-microbial peptides[12], and regulatory CD4+ T (Treg) cells[13]. While free HA or HA-based nanoparticles have been explored for treating IBD[14,15], their efficacy has been hampered by hyaluronidase-mediated rapid turnover of HA and harsh oxidative condition in inflamed colon[14,16]. On the other hand, bilirubin (BR), a hydrophobic byproduct of hemoglobin breakdown found in bile, has strong ROS-scavenging, anti-oxidant, and cytoprotective properties[17,18]; however, its clinical development has been limited due to its hydrophobicity and toxicity, and it remains unknown how to exploit the salient features of BR for treating local inflamed tissues, such as damaged colon in IBD.

Here we show that while BR is practically insoluble in water, the HA shell permitted aqueous formulation of BR and allowed targeting of orally administered HABN to inflamed colonic epithelium and pro-inflammatory macrophages via HA-CD44 interactions. Moreover, the BR core conferred HABN with hyaluronidase resistance and potent ROS-scavenging capacity, protecting colonic epithelial cells against apoptosis in a murine model of dextran sulfate sodium (DSS)-induced acute colitis - a widely used model with clinical and histological features of human ulcerative colitis, including intestinal inflammation, loss of epithelium barrier functions, dysregulated host innate immunity and gut microbiome, severe bleeding, and finally mortality[19]. Unexpectedly, our studies revealed that HABN modulated the gut microbiota, increasing its richness and diversity, and restored the expression of tight junction-associated proteins and intestinal barrier functions, thereby exerting strong anti-inflammatory effects against acute colitis.

ROS-scavenging HABN accumulates in inflamed colon

Specifically, we constructed a series of HA-BR polymers (Figure 1a, Supplementary Figures 1) and confirmed the synthesis of HA-BR conjugates using NMR (Supplementary Figure 2).

Whereas BR was insoluble in water, HA-BR conjugates with an average conjugation density of ~4 molecules of BR per each 100K HA molecule were readily dispersed in aqueous buffer (Supplementary Figure 3a,b). As shown by transmission electron microscopy and dynamic light scattering measurements, HA-BR conjugates in aqueous buffer self-assembled to form HABN (Figure 1a). As the MW of HA increased from 10 kDa to 700 kDa, the hydrodynamic size of HABN increased from 86 ± 5 nm to 416 ± 9 nm, and its zeta potential decreased from −35.6 ± 1.6 mV to −46.2 ± 5.2 mV, respectively (Supplementary Figure 3c,d). HABN exhibited significant ROS-scavenging activity ($p < 0.0001$, compared with HA and HAoxBR, an oxidized form of HABN, Figure 1b) and protected human HT-29 colonic epithelial cells from ROS-mediated cytotoxicity (Figure 1c). HABN rapidly dissociated upon exposure to ROS in the presence of a free radical, NaOCl, or a peroxy radical generator, AAPH (Supplementary Figures 4-5). In contrast, control nanoparticles self-assembled from HA-cholesterol conjugates (HACN) did not exhibit ROS-responsiveness (Supplementary Figures 6-8) and failed to protect HT-29 cells from ROS (Figure 1c), suggesting a crucial role of BR in cytoprotective effect of HABN. In addition, HABN was significantly more resistant to hyaluronidase-mediated degradation, compared with free HA (Figure 1d), potentially due to steric hinderance from self-assembled nanostructures.

Importantly, in mice given 3% DSS in drinking water as an acute model of colitis, orally administered HABN-Cy5.5 (as well as HACN-Cy5.5) accumulated in DSS-inflamed colon and associated with F4/80+ macrophages in the colonic mucosa within 6 h (Figure 1e-g, Supplementary Figures 9-10); however, HABN was not detected in the colon of healthy mice (Figure 1e-g). When HABN was incubated with murine lamina propria mononuclear cells *in vitro*, HABN was taken up by macrophages ($CD11b^+CD11c^+$ and $CD11b^+CD11c^-$) and granulocytes ($CD11b^+CD11c^-Ly6G^+$) (Supplementary Figure 11). When incubated with M0/M1/M2 J774A.1 macrophages *in vitro*, HABN was strongly associated with pro-inflammatory M1 macrophages, with minimal signal from conventional M0 or M2 macrophages (Supplementary Figure 12a,c). Pretreatment of M1 macrophages with either free HA or antibody against its known receptor, CD44, abrogated HABN signal (Supplementary Figures 12b,d), suggesting CD44-mediated association of HABN in macrophages.

Efficacy against colitis and comparison with other IBD drugs

We next evaluated the therapeutic efficacy of HABN against DSS-induced acute colitis. We first examined whether MW of HA influenced the therapeutic outcomes of HABN since the MW of HA is known to modulate pro- and anti-inflammatory responses[16]. C57BL/6 mice were given 3% DSS in drinking water for 6 days, and various HABN formulations were administered via oral gavage on days 0, 2, 4, and 6. Compared with PBS, 100K HABN treatment significantly protected animals against DSS-induced bodyweight loss and shortening of colon length, while suppressing colonic tissue damage, immune cell infiltration, and IBD-associated myeloperoxidase (MPO) activity in colon[20] (Supplementary Figure 13). In contrast, mice treated with 10K HABN or 700K HABN did not achieve full bodyweight recovery, and a subset of animals had shortened colon length.

Based on the promising outcomes of 100K HABN, we directly compared its efficacy against free 100K HA, 100K HACN, as well as PEG-BN, a control nanoparticle group with the HA moiety switched to PEG (Supplementary Figures 14-15, Figure 2a). While DSS-colitis mice treated with HABN quickly recovered their bodyweight, other control treatment groups failed to prevent the bodyweight loss (Figure 2b). Furthermore, colon length in the HABN group was similar to that in healthy mice and significantly longer than that in other treatment groups ($p < 0.01$, Figure 2c). HABN treatment also protected colonic epithelium against pathological damage and suppressed the MPO activity ($p < 0.001$, compared with PBS, Figure 2d,e). Furthermore, HAoxBR, an oxidized form of HABN, failed to protect animals against DSS-induced colitis (Supplementary Figure 16). These studies suggest that the efficacy of HABN was derived in part by both HA and BR.

We next directly compared the efficacy of HABN against other conventional IBD therapeutics widely used in the clinic, including 5-aminosalicyclic acid (5-ASA), methylprednisolone (MPS), and dexamethasone (DEX)[6]. Compared with 5-ASA, MPS, and DEX used at their clinical doses, HABN treatment exhibited significantly enhanced efficacy against DSS-induced acute colitis, achieving full bodyweight recovery, maintaining colon length, and reducing colonic damage and MPO activity (Figure 2f-j). Unlike small molecule drugs, such as MPS known for systemic side effects including thymic involution[21], HABN treatments did not trigger any overt signs of systemic toxicity, autoimmunity, or pathologies in the major organs (Supplementary Figure 17-18). We also confirmed that the free mixture of HA and bilirubin (HA+BR) had minimal therapeutic effect (Figure 2f-j). Taken together, HABN formed by self-assembled conjugates of HA and bilirubin protected animals against colitis in an effective and safe manner.

Restoration of colonic epithelium

Intrigued by these results, we examined the impact of HABN on DSS-inflamed colonic epithelium with disrupted intestinal barrier functions[1,2]. DSS-colitis mice oral administered with HABN normalized the expression patterns and mRNA levels of ZO-1 and occludin-1, tight junction-associated proteins that play pivotal roles in gut homeostasis[2] (Figure 3a,b); however, other control groups, including free HA, HACN, PEG-BN, and HA+BR treatment, had minimal impact. Furthermore, compared with other treatments, HABN prevented systemic exposure of FITC-dextran after oral administration in DSS-colitis mice ($p < 0.001$, Figure 3c), demonstrating restoration of intestinal barrier functions. HABN also induced the expression of anti-microbial peptides, including murine β-defensin 3 *in vivo* (Figure 3d). When tested in the DSS-induced model of colitis associated with ROS-mediated colonic damage[22], HABN treatment markedly reduced the level of apoptosis in the colonic epithelium, as shown by the TUNEL assay (Figure 3e). Furthermore, HABN treatment significantly reduced the local levels of pro-inflammatory cytokines, such as IL-1β, TNF-α, and IL-6 (Figure 3f), while increasing the levels of anti-inflammatory IL-10 and TGF-β cytokines (Figure 3g). Moreover, HABN treatment significantly decreased the frequencies of pro-inflammatory $CD11b^{+}Ly6C^{+}Ly6G^{-}$ monocytes and $CD11b^{+}Ly6C^{+}Ly6G^{+}$ neutrophils in lamina propria of DSS-colitis mice, while increasing the frequencies of anti-inflammatory $CD11b^{+}Ly6C^{-}Ly6G^{-}MHCII^{+}$ tissue-resident macrophages, $CD3^{+}CD4^{+}Foxp3^{+}$ regulatory T cells, and $MHCII^{+}CD11c^{+}CD11b^{-}$ DCs (Supplementary Figure 19). Notably, HABN-

mediated induction of IL-10 and TGF-β was only transient and returned to the basal levels after 10 days of stopping HABN treatment, and DSS-colitis mice treated with HABN lost the ability to accumulate HABN in colon (Supplementary Figure 20-21), suggesting normal recovery of the colon tissue.

Modulation of gut microbiome

Emerging evidence suggests the influence of gut microbiome on IBD[3-5] as well as the impact of bile organic compounds and polysaccharides on intestinal microbiota[23,24]. Thus, we examined whether HABN treatment modulated the composition of gut microbiota in DSS-colitis mice. Analyses of fecal samples by 16S rRNA gene sequencing in the V4 regions showed that HABN treatment significantly improved bacterial richness (observed OTU richness) and diversity (Shannon and inverse-Simpson indices) in DSS-colitis mice, compared with other control groups (Figure 4a,b). The non-metric multi-dimensional scaling (NMDS) plots revealed that DSS-colitis mice treated with HABN had distinct gut microbiota profile, compared with other treatment groups (Figure 4c). Further analysis at the phylum/family level showed that HABN treatment significantly increased the relative abundance of *Akkermansia muciniphila* (known to be associated with protective intestinal barrier functions[25-27]), *Clostridium* XIVα (known to induce Treg cells[28]), and *Lactobacillus* (known for beneficial roles in both IBD animal models[29-31] and IBD patients[32-35]) (Figure 4d-f), which are all key factors that are prominently decreased in IBD patients[28,32,36,37]. Interestingly, when we pre-treated DSS mice with broad-spectrum oral antibiotics, known to disrupt gut commensal microbes[38], this resulted in significantly reduced efficacy of HABN against DSS-colitis ($p < 0.05$, compared to HABN without antibiotics, Figure 4g-I, Supplementary Figure 22), suggesting that the benefits of HABN are partially attributed to modulation of gut microbiome.

Amelioration of colitis after delayed treatment

Lastly, we examined the efficacy of HABN in a setting of delayed therapy. C57BL/6 mice were given 3% DSS in drinking water for 5 days and administered with HABN three times starting day 5 (Figure 5a). Within 3 days of initiating the HABN treatment, DSS-mice started to recover bodyweight, and by day 5 of HABN treatment (day 10 of the experiment), the animals were potently protected against DSS-induced shortening of colon length, colonic damage, and MPO activity (Figure 5b-e). HABN treatment also suppressed the levels of IL-1β and TNF-α in colon while increasing the levels of anti-inflammatory IL-10 and TGF-β (Figure 5f-g).

In summary, we have developed HABN with unique anti-inflammatory properties and demonstrated its therapeutic efficacy after oral administration in a murine model of acute colitis (Figure 1a). While recent reports have explored systemic administration of polymer-modified BR for disease treatments[39-41], our work reported here demonstrate the promise of modulating intestinal barrier, microbiome, and immune responses with orally administered HABN. We show that HABN accumulated in DSS-damaged colonic epithelium and pro-inflammatory macrophages (Figures 1e-g) and upregulated the expression levels of tight junction-associated proteins and anti-microbial peptides in colon, while restoring intestinal

barrier functions and protecting the epithelial layer against apoptosis (Figure 3a-e). Additionally, HABN treatment had a potent immune-modulatory impact in the lamina propria, characterized by significant decreases in pro-inflammatory cytokines and immune cells with concomitant increases in anti-inflammatory factors (Figure 3f-g, Supplementary Figure 19). Moreover, HABN promoted rapid recovery from bodyweight loss, inhibited colon and mucosa damage, and decreased colonic MPO activity in the DSS murine model of acute colitis, whereas other control groups, including free HA mixed with bilirubin, HACN, as well as an oxidized form of HABN, HAoxBR, failed to protect animals against colitis (Figure 2, Supplementary Figure 16). In addition, PEG-BN, which had shown good efficacy against colitis after intravenous administration in a previous study[39], exerted only a moderate effect after oral administration in this study (Figure 2), potentially due to the lack of HA-mediated targeting of inflamed colon. Importantly, HABN alleviated the symptoms of colitis more effectively than other conventional IBD therapies used in the clinic, such as 5-ASA, MPS, and DEX (Figure 2f-j). While adverse events, such as opportunistic infections, autoimmunity, and liver toxicity, are associated with conventional immunosuppressive agents[6,10], we did not observe any overt toxicity after repeat HABN treatments, and HABN only transiently elevated local levels of anti-inflammatory IL-10 and TGF-β, which returned to the basal levels after stopping the HABN treatment (Supplementary Figure 18 & 20). Taken together, these results show the efficacy and safety of HABN and demonstrate that both the HA shell and the BN core play critical and complementary roles in multi-faceted benefits of HABN against colitis.

HABN also altered the gut microbiome, increasing the diversity and relative abundance of *Akkermansia muciniphila, Clostridium* XIVα, and *Lactobacillus* (Figure 4). In particular, IBD patients have dramatically decreased abundance of *Akkermansia muciniphila*, known to promote mucus production and expression of tight junction proteins[25-27]; *Clostridium* XIVα whose metabolic byproduct, butyrate, induces Treg cells in lamina propria[28]; and *Lactobacillus*, known to exert anti-inflammatory effects in both animal models of colitis[29-31] and IBD patients[32-35]. Notably, when we depleted commensal gut microbes with broad-spectrum oral antibiotics, HABN therapy partially lost its efficacy against DSS-colitis (Figure 4g-i). While we speculate that the therapeutic efficacy of HABN was mediated in part by changes in the gut microbiome, further investigation is warranted to understand the role of altered microbiome on colitis. In addition, our current studies are limited to the mouse model of DSS-induced acute colitis, and validation in other advanced pre-clinical models of IBD is needed. Overall, these results suggested that ROS-responsive and hyaluronidase-resistant HABN accumulated in DSS-inflamed colon and protected colonic epithelium against inflammation while restoring disrupted intestinal barrier functions and gut microbiome.

It is increasingly recognized that the gut microbiome has a crucial role in human health, and the dysregulated microbiome has been implicated in a number of human diseases, including IBD, obesity, diabetes, cancer, and neurological disorders[3,42,43]. In particular, inorganic nanoparticles, such as silver nanoparticles widely used for their antimicrobial properties in consumer products and pharmaceutical products, have been shown to disrupt the gut microbiome, thus raising awareness of nanotoxicology and unintended outcomes of nanotechnology[44-46]. While a recent study has reported a nanogel system that can overcome

the dysregulated gut microbiome for vaccine applications in a mouse model of metabolic syndrome[47], our work represents, to the best of our knowledge, the first demonstration of oral nanomedicine capable of targeting inflamed colon and directly modulating the intestinal barrier and gut microbiota while exerting potent anti-inflammatory responses against colitis. As dysregulated gut microbiota and intestinal barrier functions are highly associated with systemic diseases, our strategy described here may offer a convenient yet powerful platform for treatment of other inflammatory diseases.

Methods

Synthesis of hyaluronic acid-bilirubin conjugate (HA-BR) and hyaluronic acid-cholesterol conjugate (HA-Chol).

Before synthesizing hyaluronic acid-bilirubin conjugate (HA-BR), an acid form of hyaluronic acid (HA) from hyaluronic acid sodium salt (Lifecore Biomedical) and an aminoethylene-bilirubin conjugate (AE-BR) were prepared. The acidic form of hyaluronic acid (HA) from hyaluronic acid sodium salt was prepared by dialysis against 0.01M HCl for overnight followed by lyophilization. AE-BR was prepared as previously described with modifications[48]. Briefly, 750 μmol of bilirubin (Lee Biosolutions) and 520 μmol of N-hydroxysuccinimide (NHS, Sigma-Aldrich) were added to 7.5 ml of dimethyl sulfoxide (DMSO) containing 0.225 μl of trimethylamine (TEA). Subsequently, 337.5 μmol of EDC [1-Ethyl-3-(3-dimethylaminopropyl)carbodiimide] (Sigma-Aldrich) was added to the mixture. After stirring for 10 min at room temperature (RT), 562.5 μmol of ethylenediamine (EDA) was added to the mixture, and the reaction was allowed to proceed with stirring for 4 h at RT under nitrogen gas. 50 ml of chloroform was added to the mixture and then washed twice with 50 ml of 0.1M HCl, 0.1M NaHCO3 and then water. After evaporating the chloroform solution, 45 ml of methanol was added to the reaction mixture and then centrifuged at 3,000 x g for 10 min. The supernatant was then evaporated to yield AE-BR.

To synthesize hyaluronic acid-bilirubin conjugate (HA-BR) or hyaluronic acid-cholesterol conjugate (HA-Chol), 80 μmol of an acidic form of HA, 40 μmol of NHS were added to 4.8 ml of DMSO and then, after adding of 140 μmol of EDC to the mixture, the mixture was stirred for 10 min at RT. Subsequently, 20 μmol of AE-BR, or 5 μmol of cholesterol-PEG-NH2 (Nanosoft Polymers) was mixed with the mixture for overnight at RT under nitrogen gas. The mixture was slowly poured into 30 ml of 0.01M NaOH and then dialysis was performed against 0.01M NaOH for 5 hr. Further dialysis was performed against 1:1 ratio of water/acetonitrile three times for 1 day, followed by distilled water three times for 2 days. The resulting solution was finally lyophilized, yielding HA-BR (native sodium salt form; 26.5 μg/ml of BR in 1mg/ml of HABN) or HA-chol. ^{1}H-NMR spectra were obtained on a Varian 500MHz system (Varian); chemical shifts represent ppm downfield from tetramethylsilane. Bilirubin portion of HABN was calculated by measurement of UV/VIS spectra using Synergy™ NEO HTS multi-mode microplate reader (BioTek Instruments Inc).

Synthesis of PEGylated bilirubin (PEG-BR).

PEG-BR was prepared as previously described with modifications[48]. 75 μmol of bilirubin and 33.75 μmol of EDC were added to 0.6 ml of DMSO containing 225 μl of TEA and 52

μmol of NHS for 10 min at RT. After then, 15 μmol of polyethylene glycol 20K-amine (PEG-NH2, Nanocs) and the mixture was mixed for 4 h under nitrogen gas. Subsequently, the mixture was added to 50 ml of chloroform and then the organic solvents were washed by 50 ml of 0.1M HCl twice, followed by washing with 50 ml of 0.1M NaHCO3 twice and finally washed with 50 ml of distilled water twice. The organic layer was evaporated, and 50 ml of methanol was added to the residue. After centrifugation at 3,000 x g for 10 min, the supernatant was collected and then evaporated. Dialysis was performed as described in the previous section. To yield PEGylated bilirubin (PEG-BR), lyophilization was performed. The final structure was confirmed by ^{1}H-NMR. ^{1}H-NMR spectra were recorded on a Varian 500MHz system; chemical shifts represent ppm downfield from tetramethylsilane.

Synthesis of HA-Cy5.5 conjugate, HA-Chol-Cy5.5 conjugate, and HA-BR-Cy5.5 conjugate.

Prior to conjugating HA-BR or HA-Chol with Cy5.5 amine (AAT Bioquest), a native sodium salt form of HA-BR, HA-Chol or free HA was converted into an acidic form of HA-BR, HA-Chol or free HA by dialysis processes for efficient dissolution to DMSO. 10 μmol of each power form was dissolved into 5 ml of distilled water. Dialysis was performed against 0.1M HCl for overnight and then the solution was dialyzed against distilled water three times for 1 day. The resulting powder was obtained through a lyophilization step. 10.5 μmol of the acidic form of HA-BR, HA-Chol or free HA was dissolved in 0.8 ml of DMSO for overnight. 2 μmol of NHS and 2 μmol of EDC were added to the mixture. After mixing for 10 min at RT, 0.1 μmol of Cy5.5-NH2 was further added to the reaction mixture. After stirring for overnight at RT, dialysis was performed once more against 0.01M NaOH three times for 1 day, followed by distilled water twice for 2 day. After lyophilization, the native sodium salt form of HA-Cy5.5 conjugate, HA-Chol-Cy5.5 conjugate, or HA-BR-Cy5.5 conjugate was obtained.

Preparation of Cy5.5-tagged hyaluronic acid-bilirubin nanoparticles (HABN), hyaluronic acid-cholesterol nanoparticles (HACN), or PEGylated bilirubin nanoparticles (PEG-BN).

After dissolving HA-BR, HA-Chol, PEG-BR, HA-BR-Cy5.5 or HA-Chol-Cy5.5 in water or PBS, ultra-sonication (140W, 26Hz, 2s on 3s off of short interval) was performed for 5 min at 4°C. After filtration through a 0.45 μm of filter membrane, even size of hyaluronic acid-bilirubin nanoparticles (HABN), hyaluronic acid-cholesterol nanoparticles (HACN), PEGylated bilirubin nanoparticles (PEG-BN), Cy5.5 conjugated hyaluronic acid-bilirubin nanoparticles (HABN-Cy5.5) or Cy5.5 conjugated hyaluronic acid-cholesterol nanoparticles (HACN-Cy5.5) were acquired. The size and zeta potential of the nanoparticles were obtained using a Nanosizer ZS90 (Malvern Instruments Ltd). Morphology was examined by Transmission Electron Microscopy (TEM) using JEOL 1400-plus TEM (JEOL USA). The resulting nanoparticles were diluted in PBS or culture medium for *in vitro* and *in vivo* experiments.

ROS-responsiveness of 100K HABN and 100K HACN.

100K HABN or 100K HACN in PBS was incubated with or without a 100 mM solution of a peroxy radical-generating reagent AAPH [2,2'-Azobis(2-amidinopropane) dihydrochloride] (Sigma-Aldrich, St. Louis, MO), 5 mM solution of hydrogen peroxide (H2O2, Sigma-Aldrich) or 1 mM solution of sodium hypocholrite (NaOCl, Sigma-Aldrich) for 1 h at 37°C.

The hydrodynamic size of the 100K HABN or 100K HACN were monitored at predetermined times and DLS, respectively. The reaction was also monitored for 1 h by measuring absorbance at 453 nm using Synergy™ NEO HTS multi-mode microplate reader.

Fluorescence measurement of DCFDA (dichlorofluorescin diacetate) upon ROS and HABN.

50 μM of DCFDA in PBS was incubated with 1 mM of AAPH in the presence of BR (50 μM), HA (1 mg/ml), HABN (1 mg/ml), or PBS. Fluorescence signals of fluorescent 2',7'-dichlorofluorescein (DCF) generated from DCFDA by oxidation were monitored for 1 h at 37°C using Synergy™ NEO HTS multi-mode microplate reader at 490 nm excitation and 520 nm emission.

Preparation of a native polymer form of oxidized hyaluronic acid-bilirubin fragments (HAoxBR).

For acquiring a native polymer form of oxidized hyaluronic acid-bilirubin fragments (HAoxBR), 100K HABN in water was incubated with a 100 mM solution of AAPH for 1 hr at 37°C. After the reaction, the solution was centrifuged with Amicon Ultra-Centrifugal filter with a membrane of 10 kDa at 17,500 x g at 4°C for 15 min three times for removing remaining AAPH. The filtered solution was lyophilized, to yield HAoxBR.

Colorimetric assessment of terminal N-acetyl-D-glucosamine (Hyaluronan breakdown products).

N-acetyl-D-glucosamine (NAG), a breakdown product of HA after exposure to hyaluronidase (HYAL), was measured using a colorimetric method described previously by Reissig et al[49]. Briefly, 100K HABN (1 mg/ml), or 100K HA (1 mg/ml) in pH 6.0 PBS buffer was treated with 100 lU/ml of HYAL II (Sigma-Aldrich) at 37°C for 6 h. 1 mg/ml of N-acetyl-D-glucosamine was used for control group. At determined time point (0 h, 10 min, 0.5 h, 1 h, 2 h, 4 h and 6 h), 100 μl of the samples were diluted up to 0.5 ml of PBS and heated for 5 min at 100°C to stop the enzyme reaction. After then, 0.1 ml of 0.8M potassium tetraborate (pH 9.0) was added to the mixture and further heated for 3 min at 100°C and cooled in tap water. 3 ml of p-dimethylaminobenzaldehyde (DMAB) reagent (10 g of DMAB dissolved in 100 ml of glacial acetic acid containing 12.5 % (v/v) of 10M HCl) were then added and immediately after mixing, the tubes were placed in a water bath at 37°C. After 20 min, the solution was measured at 544 nm wavelength using Synergy™ NEO HTS multi-mode microplate reader.

Preparation of Nile red-loaded 100K HABN.

10 μl of 1.5 mg/ml of Nile red (Sigma-Aldrich) in Methanol was added to 500 μl of 1mg/ml of 100K HABN in water and then, ultra-sonication (140W, 26Hz, 2s on 3s off of short interval) was performed for 5 min at 4°C. After moderate magnetic stirring for overnight at RT to evaporate any remaining organic solvent, filtration through a 0.45 μm of filter membrane was performed to remove remaining unloaded aggregated Nile red, yielding even size of Nile red loaded 100K HABN (Nile red@100K HABN). Loaded amount of Nile red in the nanoparticles were measured by high performance liquid chromatography (HPLC).

Animals.

Animals were cared for following federal, state, and local guidelines. All work performed on animals was in accordance with and approved by the Institutional Animal Care & Use Committee (IACUC) at University of Michigan, Ann Arbor. All animals were obtained from the Jackson Laboratory (Bar Harbor, ME) as mixed littermates and housed under pathogen-free conditions in the animal facility at the North Campus Research Complex of University of Michigan. Mice were co-housed for a week before random assignment to experimental groups in order to synchronize the gut microbiome among individual mice and reduce the heterogeneity of it[50]. The investigators were not blinded to allocation during experiments and outcome assessment unless each section particularly includes any blind assessment.

DSS-induced model of colitis.

Six-weeks old female C57-BL/6 mice were housed in groups of five mice per cage and acclimatized for 1 wk before inclusion in the study. Mice received 3% Dextran Sodium Sulfate (DSS, 40kDa; Alfa Aesar) supplemented in the drinking water 5 or 6 days, followed by normal water. Control healthy mice were provided with normal water only. 30 mg/kg of HA (10kDa, 100kDa, 700kDa, or 1500kDa), , 30 mg/kg of HAoxBR, 30 mg/kg of HABN (10kDa, 100kDa, or 700kDa), 30 mg/kg of PEG-BN, 30 mg/kg of HACN, HA+BR mixture (equivalent dose of HA and BR of HABN), 1 mg/kg of MPS, 1 mg/kg of DEX, 40 mg/kg of 5-ASA or PBS was administered via an oral route into mice on predetermined days. In some experiments, we pre-treated mice by administering a cocktail of antibiotics (ampicillin 1 g/L, vancomycin 0.5 g/L, neomycin 1 g/L, metronidazole 1 g/L) in drinking water for 5 days before DSS treatment. Changes in bodyweight were assessed daily over the 9 or 10 d experimental period. Feces were collected on the predetermined day for microbiome analysis. On the last day of the experiment, mice were sacrificed, and the entire colon was excised. Colon length was measured and gently washed with physiological saline. Then, two pieces of 0.5 cm of the distal section were used for histological assessment and immunofluorescence staining, respectively. The remaining colon tissue samples were used for FACS analysis and determining MPO activity and the concentrations of cytokines.

Histology.

For histological analyses, H&E colonic tissue sections were prepared by ULAM in-vivo animal core. Briefly, a 1 cm section of the distal colon was first fixed by incubation with 4% (v/v) buffered formalin and 70% (v/v) alcohol and embedded in paraffin. Tissue sections of the distal colon were then prepared, stained with H&E and analyzed by Mantra™ quantitative pathology workstation (PerkinElmer). The severity of colonic histological damage was scored in a blinded fashion to prevent observer bias, as previously described[39]. Briefly, colonic damage was assigned scores as follows: 0, normal; 1, hyperproliferation, irregular crypts, and goblet cell loss; 2, mild to moderate crypt loss (10–50%); 3, severe crypt loss (50–90%); 4, complete crypt loss, surface epithelium intact; 5, small- to medium-sized ulcers (<10 crypt widths); 6, large ulcers (≥10 crypt widths). Inflammatory cell infiltration was scored separately for the mucosa (0, normal; 1, mild; 2, modest; 3, severe), submucosa (0, normal; 1, mild to modest; 2, severe), and muscle/serosa (0, normal; 1,

moderate to severe). Scores for epithelial damage and inflammatory cell infiltration were summed, resulting in a total scoring range of 0 to 12.

MPO activity measurement.

MPO activity was determined as previously described[39]. Briefly, a colon segment (1:10 w/v) in 50 mM phosphate buffer (pH 6.0) was homogenized using an IKA T25 ULTRA-TURRAX basic homogenizer (IKA® Works, Inc., Wilmington, NC) at 4°C. The colon suspension was 10 fold-diluted with 50 mM phosphate buffer containing 0.5% hexadecyltrimethylammonium bromide (HTAB, Sigma-Aldrich). After sonicating for 10 s and subjecting to three freeze-thaw cycles, each sample was centrifuged at 17,000 x g for 5 min. A 10 μl of each supernatant was then added to 290 μl of 50 mM phosphate buffer (pH 6.0) containing 0.167 mg/ml of o-dianisidine dihydrochlrodie (Sigma) and 0.005% H_2O_2, and changes in absorbance at 460 nm were measured over 5 min. The protein concentration of the supernatant sample was measured using a Micro BCA Protein Assay Kit (Thermo Fisher Scientific). MPO activity was determined by comparison to a standard MPO curve (Sigma-Aldrich).

In vivo ELISA analysis.

For determining the concentrations of cytokines in the colon tissue, the colon segment in 50 mM phosphate buffer (pH 6.0) was homogenized (1:10 w/v) using an IKA T25 ULTRA-TURRAX basic homogenizer (IKA® Works, Inc.) at 4°C. Each sample was centrifuged for 10 min at 10,000 × g at 4°C. The levels of cytokines in the resulting supernatants or medium were measured by enzyme-linked immunosorbent assay (ELISA) at the Cancer Center Immunology Core of the University of Michigan.

In vivo immunofluorescence imaging.

For acquiring *in vivo* confocal microscopy images, 5 cm of colon tissue was placed in OCT cryomold blocks and transferred to −70°C freezer. Tissue sections of the distal colon from the OCT embedded frozen blocks were fixed with 4% PFA, permeabilized with 0.1% or 0.25 % Triton X-100 and blocked with PBST containing 1% or 3% BSA and 22.52 mg/ml of glycine. The sections were stained with 1 μg/ml of murine anti-beta defensin 3 (ortholog of human beta-defensin 2) polygonal rabbit antibody for 1 hr followed by 2 μg/ml of anti-rabbit secondary antibody conjugated with AlexaFluor-594, 5 μg/ml of anti-F4/80 antibody conjugated with AlexaFluor-488, 5 μg/ml of anti-beta-catenin antibody conjugated with AlexaFluor-594 or 2 μg/ml of anti-EpCAM antibody conjugated with AlexaFluor-594, or 5 μg/ml of anti ZO-1 antibody conjugated with AlexaFluor-488 and 1 μg/ml of anti Occludin-1 antibody conjugated with AlexaFluor-594. Nuclei were counter-stained with Hoechst 33342. Images of random fields of view were acquired by confocal laser-scanning microscopy (Nikon A1; Nikon Instruments Inc, Melvile, NY). Terminal deoxynucleotidyl transferase (TdT) dUTP Nick-End Labeling (TUNEL) assay was performed to detect apoptosis in OCT-embedded frozen blocks according to the manufacturer's instruction.

Quantitative real-time PCR.

RNA was extracted from colonic tissues using the E.Z.N.A.® Total RNA Kit I (Omega Bio-tek) according to the manufacturer's protocol. Reverse transcription was performed using the High-Capacity cDNA Reverse Transcription Kit (Thermo Fisher Scientific). Quantitative PCR was performed with SYBR Green qPCR Kits (Alkali Scientific). The cycling conditions were 95 °C for 3 min and then 40 cycles of 95 °C for 15 s, 60 °C for 1 min. The relative expression of target genes was calculated using β-actin as a reference gene. The following primer sets were used for amplifications: ZO-1-Fw; 5'-CTTCTCTTGCTGGCCCTAAAC-3', ZO-1-Rv; 5'-TGGCTTCACTTGAGGTTTCTG-3', occludin-Fw; 5'-CACACTTGCTTGGGACAGAG-3', occludin-Rv; 5'-TAGCCATAGCCTCCATAGCC-3', β-actin-Fw; 5'-AAGTGTGACGTTGACATCCG −3', and β-actin-Rv; 5'-GATCCACATCTGCTGGAAGG −3'.

In vivo intestinal permeability assay.

In vivo assay of intestinal permeability was performed using an FITC-dextran, as described previously[19]. Briefly, mice were deprived of food and water for 4 h and then orally gavaged with 0.6 mg/g body weight of 4 KDa FITC-dextran (FD4, Sigma). Blood was collected retro-orbitally after 3 h, and FITC fluorescence intensity was measured in the serum samples (excitation, 485 nm; emission, 520 nm). FITC-dextran concentrations were determined using a standard curve generated by serial dilution of FITC-dextran in mouse serum.

Isolation of intestinal lamina propria mononuclear cells (LPMCs).

Colon was removed and placed in cold Ca^{2+}, Mg^{2+}-free Hank's balanced salt solution (HBSS; Gibco). After removal of the mesentery, the colon was opened longitudinally, thoroughly washed in HBSS and cut into small pieces. The dissected mucosa was incubated with HBSS containing 1 mM dithiothreitol (Sigma-Aldrich) and 5 mM EDTA (Quality biological) for 30 min at 37°C to remove the epithelial layer. The pieces of intestine were washed and placed in HBSS containing 1.5% FBS, 200 U/mL collagenase Type 3 and 0.01 mg/mL DNase (all Worthington Biochemical Corporation) for 1 h at 37°C. The digested tissues were washed, resuspended in 40% Percoll (GE Healthcare) and overlaid on a 75% Percoll fraction. Percoll gradient separation was performed by centrifugation at 700 × g for 20 min at room temperature. Mononuclear cells were collected at the interphase, washed, and resuspended in staining buffer containing PBS, 0.5% BSA, 2 mM EDTA for flow cytometry or RPMI-1640 medium (Sigma-Aldrich) containing 10% FBS.

Flow Cytometry.

Cells were pre-incubated with a FcγR-blocking mAb (CD16/32; 2.4G2, BD Bioscience) for 20 min followed by incubation with specific mAbs for 20 min on ice. After staining surface molecules, the cells were re-suspended in fixation/permeabilization solution (eBioscience), and intracellular staining of FOXP3 was performed with a FOXP3 staining buffer kit (eBioscience). Flow cytometric analyses were performed on a LSR II system (Becton Dickinson), and data were analyzed using Flowjo software (Tree Star). Background fluorescence was assessed by staining with isotype-matched control mAbs. FITC-, PE-, PerCP-Cy5.5-, APC-, PE-Cy7-, APC-Cy7- or AlexaFluor 647-conjugated mAbs against

CD4 (GK1.5), CD3 (145-2C11), CD11b (M1/70), CD11c (N148), Ly6c (HK1.4), MHCII (M5/114.15.2), 7AAD and FOXP3 (FJK-16S) were from eBioscience, CD45 (30-F11) and Ly6G (1A8) were from Invitrogen.

Microbiome analysis.

1 pellet of feces was added to each well of PowerMag Glass Bead plate (Qiagen). The plate was properly packaged and shipped to the University of Michigan Medical School Host Microbiome Initiative (HMI) and all the processes showed in the below were performed by the HMI. Genomic DNA was extracted by using the Qiagen MagAttract Power Microbiome kit DNA/RNA kit (Qiagen, catalog no. 27500-4-EP) on the EpMotion 5075 (Eppendorf) liquid handler. Extracted DNA were then used to generate 16S rRNA libraries for community analysis[51] using the MiSeq Illumina sequencing platform. Barcoded dual-index primers specific to the V4 region of the 16S rRNA gene were used for the construction.

Sequences were curated using the community-supported software program mothur (v.1.39)[52] and by following the steps outlined in the MiSeq SOP (http://www.mothur.org/wiki/MiSeq_SOP)[53]. Sequences were assigned to operational taxonomic units (OTUs) using a cut-off value of 0.03 and classified against the Ribosomal Database Project 16S rRNA gene training set (version 9) using a naive Bayesian approach with an 80% confidence threshold. Curated OTU sequence data were converted to relative abundance ± SEM. The Shannon diversity and inverse Simpson indices were used to calculate alpha diversity, and the Yue and Clayton dissimilarity metric was used for beta diversity measures. Analysis of molecular variance (AMOVA) was used to detect significant clustering of different treatment groups in nonmetric multidimensional scaling (NMDS). To confirm what specific bacterial taxa are over-and/or under-represented among groups, we analyzed relative abundance results by using linear discriminant analysis effect size (LEfSe).

In vivo IVIS imaging.

To check ability of HABN to target the inflamed site in the colon, a 1 day after preparing colitis mice or heathy mice by giving 3% DSS water or normal water for five days, 7.5 mg/kg (0.3% 1.8 μg Cy 5.5;) of HABN-Cy5.5, HACN-Cy5.5, or HA-Cy5.5 was orally administered into the mice. After 6 h, mice were euthanized, and organs including heart, kidney, lung, spleen, liver, stomach, small intestine and colon were excised. Fluorescence intensities in organs from each group were analyzed using a Xenogen IVIS Lumina *in vivo* imaging system (PerkinElmer) with a Cy 5.5 filter channel and an exposure time of 5 s.

Cell culture.

J774A.1 murine macrophage and HT-29 colonic epithelial cell lines were obtained from the American Type Culture Collection (ATCC, All cell lines have been tested negative for mycoplasma contamination. J774A.1 cells or HT-29 cells in DMEM medium (Gibco™) containing 10% (v/v) heat-inactivated fetal bovine serum (FBS), 100 IU/ml penicillin/streptomycin, and L-glutamine were cultured in a humidified 5% CO_2 atmosphere at 37°C.

In vitro analysis of LPMCs.

For the uptake study with LPMCs, LPMCs were isolated from the colon as described in the "Isolation of intestinal lamina propria lymphocytes" section. LPMCs were cultured with 10 μg/ml of 100K HABN-Cy 5.5 for 3 h at 37°C and then, cells were pre-incubated with a FcγR-blocking mAb (CD16/32; 2.4G2, BD Bioscience) for 20 min, followed by incubation with specific mAbs for 20 min on ice as detailed in the "Flow cytometry" section. Flow cytometric analyses were performed on a LSR II system, and data were analyzed using Flowjo software.

In vitro confocal microscopy.

For the uptake study with the J774A.1 murine macrophage cell line, J774A.1 cells in culture medium were seeded onto cover slip in 24-well plates (5×10^3/well). After incubation for 2 days at 37°C, the cells were treated with 100 ng/ml of LPS and 10 ng/ml of IFN-γ for M1 induction, 20 ng/ml of IL-4 for M2 induction for 24 h, or control medium. 5 μg/ml of 100K HABN-Cy5.5, 100 ng/ml of Nile Red, Nile Red@100K HABN (Nile Red, 100 ng/ml; 100K HABN 2.5 μg/ml), or control medium was treated with the cells for 1 h. The cells were then fixed with 4% PFA for 5 min, counter-stained with Hoechst 33342 for 10 min and analyzed by confocal laser-scanning microscopy. For completion study, 5 mg/ml of free HA or 500 μg/ml of anti-CD44 antibody was pre-treated with the cells for 30 min before nanoparticle treatment.

In vitro immunofluorescence imaging.

For comparing β-defensin 2 levels on HT-29 colonic epithelial cells, HT-29 cells in culture medium were seeded onto 24 well plates (5×10^4/well). After incubation for 2 days, 30 μg/ml of 100K HABN, 100K HA, 100K HACN, 20K PEG-BN or control medium were treated with the cells for 24 h. The cells were fixed and permeabilized with 4% PFA for 10 min and then 0.1% Triton X-100 for 10 min, blocked with PBST containing 3% BSA for 1 h, stained with anti-β-defensin 2 (human reactivity) rabbit polyclonal antibody (1 μg/ml), followed by 2 μg/ml of anti-rabbit IgG secondary antibody conjugated with AlexaFlour 488, and the counter-stained with Hoechst 33342. Images of random fields of view were acquired by confocal laser-scanning microscopy.

CCK-8 assay.

HT-29 cells in culture medium were grown in 96-well plates (0.7×10^4/well) for 24 h at 37°C. After medium was removed, fresh medium, H_2O_2 (100 μM), or different concentrations of HABN (500 μg/ml), HACN (500 μg/ml), HA (500 μg/ml), with or without H_2O_2 (100 μM), was added to each well and plates were incubated for 24 h. After incubation, cells were washed with fresh culture medium and 100 μl of fresh culture medium was added to each well, followed by the addition of 10 μl of CCK-8 (Dojindo Molecular Technologies. Inc.) and after incubation for 1 h at 37°C, the absorbance was measured at 450 nm using a 96-well plate microreader.

In vivo toxicity test.

Six-weeks old female C57-BL/6 mice were housed in groups of five mice per cage and acclimatized for 1 wk before inclusion in the study. 30 mg/kg of HABN (10 kDa, 100 kDa, or 700 kDa) or PBS was administered via an oral route on day 0, 2, 4, and 6. Mice were observed over a 1 wk period for changes in behavior or weight. Blood was collected from jugular vein and immediately sent to the ULAM Pathology Core for Animal Research for blind blood assessment. Mice were sacrificed, and their major organs (heart, liver, lung, kidney, spleen, and colon) were collected for histopathological analysis. Each organ was fixed with 4% (v/v) buffered formalin and 70% (v/v) alcohol, and embedded in paraffin. Tissues were sectioned, stained with H&E, and examined by microscopy. All histological assessments were performed in a blinded manner to prevent observer bias.

Statistical analysis.

All experiments were performed at least twice with duplicate repeated measures. The results are expressed as means ± s.e.m. A one-way or two-way ANOVA, followed by Tukey's HSD multiple comparison post hoc test was used for testing differences among groups. Data were approximately normally distributed and variance was similar between the groups. Experiments were repeated multiple times as independent experiments as indicated in the figure captions. Shown in the figure is a complete dataset from one representative, independent experiment. No samples were excluded from analysis. Statistical significance is indicated as $*p < 0.05$, $**p < 0.01$, $***p < 0.001$, and $****p < 0.0001$. GraphPad Prism 6.0 (GraphPad Software, La Jolla, CA) was used for statistical analyses.

Reporting Summary.

Further information on research design is available in the Nature Research Reporting Summary linked to this article.

DATA AVAILABILITY

The authors declare that data supporting the findings of this study are available within the article and its Supplementary Information files. All relevant data can be provided by the authors upon reasonable request.

Supplementary Material

Refer to Web version on PubMed Central for supplementary material.

Acknowledgments

This work was supported in part by NIH (R01EB022563, R01AI127070, R01CA210273, R01CA223804, U01CA210152, R01DK108901), MTRAC for Life Sciences Hub, and Emerald Foundation. J.J.M. is a Young Investigator supported by the Melanoma Research Alliance (348774), DoD/CDMRP Peer Reviewed Cancer Research Program (W81XWH-16-1-0369), and NSF CAREER Award (1553831). Opinions interpretations, conclusions, and recommendations are those of the author and are not necessarily endorsed by the Department of Defense. The authors thank Dr. Hayashi Atsushi for his technical help with LPMC isolation and flow cytometric analysis; the University of Michigan Medical School Host Microbiome Initiative for microbial community analysis; the University of Michigan Cancer Center Immunology Core for ELISA analysis; the ULAM (Unit for Laboratory Animal Medicine) In Vivo Animal Core (IVAC) for tissue sectioning and histological analysis of colon samples; the

ULAM Pathology Core for blood analysis; and the College of Pharmacy Biochemical NMR Core at the University of Michigan.

REFERENCES

1. Turner JR Intestinal mucosal barrier function in health and disease. Nat Rev Immunol 9, 799–809 (2009). [PubMed: 19855405]
2. Citi S Intestinal barriers protect against disease. Science 359, 1097–1098 (2018). [PubMed: 29590026]
3. Round JL & Mazmanian SK The gut microbiota shapes intestinal immune responses during health and disease. Nat Rev Immunol 9, 313–323 (2009). [PubMed: 19343057]
4. Kostic AD, Xavier RJ & Gevers D The microbiome in inflammatory bowel disease: current status and the future ahead. Gastroenterology 146, 1489–1499 (2014). [PubMed: 24560869]
5. Halfvarson J, et al. Dynamics of the human gut microbiome in inflammatory bowel disease. Nat Microbiol 2, 17004 (2017). [PubMed: 28191884]
6. Bernstein CN, et al. World Gastroenterology Organization Practice Guidelines for the diagnosis and management of IBD in 2010. Inflamm Bowel Dis 16, 112–124 (2010). [PubMed: 19653289]
7. Lautenschlager C, Schmidt C, Fischer D & Stallmach A Drug delivery strategies in the therapy of inflammatory bowel disease. Adv Drug Deliv Rev 71,58–76 (2014). [PubMed: 24157534]
8. Wilson DS, et al. Orally delivered thioketal nanoparticles loaded with TNF-alpha-siRNA target inflammation and inhibit gene expression in the intestines. Nat Mater 9, 923–928 (2010). [PubMed: 20935658]
9. Zhang S, et al. An inflammation-targeting hydrogel for local drug delivery in inflammatory bowel disease. Sci Transl Med 7, 300ra128 (2015).
10. Stallmach A, Hagel S & Bruns T Adverse effects of biologics used for treating IBD. Best Pract Res Clin Gastroenterol 24, 167–182 (2010). [PubMed: 20227030]
11. Rayahin JE, Buhrman JS, Zhang Y, Koh TJ & Gemeinhart RA High and low molecular weight hyaluronic acid differentially influence macrophage activation. ACS Biomater Sci Eng 1, 481–493 (2015). [PubMed: 26280020]
12. Hill DR, Kessler SP, Rho HK, Cowman MK & de la Motte CA Specific-sized hyaluronan fragments promote expression of human beta-defensin 2 in intestinal epithelium. J Biol Chem 287, 30610–30624 (2012). [PubMed: 22761444]
13. Bollyky PL, et al. Intact extracellular matrix and the maintenance of immune tolerance: high molecular weight hyaluronan promotes persistence of induced CD4+CD25+ regulatory T cells. J Leukoc Biol 86, 567–572 (2009). [PubMed: 19401397]
14. Zheng L, Riehl TE & Stenson WF Regulation of colonic epithelial repair in mice by Toll-like receptors and hyaluronic acid. Gastroenterology 137, 2041–2051 (2009). [PubMed: 19732774]
15. Xiao B, et al. Combination Therapy for Ulcerative Colitis: Orally Targeted Nanoparticles Prevent Mucosal Damage and Relieve Inflammation. Theranostics 6, 2250–2266 (2016). [PubMed: 27924161]
16. Petrey AC & de la Motte CA Hyaluronan, a crucial regulator of inflammation. Front Immunol 5, 101 (2014). [PubMed: 24653726]
17. Kapitulnik J Bilirubin: an endogenous product of heme degradation with both cytotoxic and cytoprotective properties. Mol Pharmacol 66, 773–779 (2004). [PubMed: 15269289]
18. Sedlak TW, et al. Bilirubin and glutathione have complementary antioxidant and cytoprotective roles. Proc Natl Acad Sci U S A 106, 5171–5176 (2009). [PubMed: 19286972]
19. Chassaing B, Aitken JD, Malleshappa M & Vijay-Kumar M Dextran sulfate sodium (DSS)-induced colitis in mice. Curr Protoc Immunol 104, Unit 15 25 (2014).
20. Hansberry DR, Shah K, Agarwal P & Agarwal N Fecal Myeloperoxidase as a Biomarker for Inflammatory Bowel Disease. Cureus 9, e1004 (2017). [PubMed: 28286723]
21. Hall ED, McCall JM, Chase RL, Yonkers PA & Braughler JM A nonglucocorticoid steroid analog of methylprednisolone duplicates its high-dose pharmacology in models of central nervous system trauma and neuronal membrane damage. J Pharmacol Exp Ther 242, 137–142 (1987). [PubMed: 3039107]

22. Li B, Alli R, Vogel P & Geiger TL IL-10 modulates DSS-induced colitis through a macrophage-ROS-NO axis. Mucosal Immunol 7, 869–878 (2014). [PubMed: 24301657]
23. Gibson GR, et al. Expert consensus document: The International Scientific Association for Probiotics and Prebiotics (ISAPP) consensus statement on the definition and scope of prebiotics. Nat Rev Gastroenterol Hepatol 14, 491–502 (2017). [PubMed: 28611480]
24. Ma C, et al. Gut microbiome-mediated bile acid metabolism regulates liver cancer via NKT cells. Science 360(2018).
25. Cani PD & de Vos WM Next-Generation Beneficial Microbes: The Case of Akkermansia muciniphila. Front Microbiol 8, 1765 (2017). [PubMed: 29018410]
26. Everard A, et al. Cross-talk between Akkermansia muciniphila and intestinal epithelium controls diet-induced obesity. Proc Natl Acad Sci U S A 110, 9066–9071 (2013). [PubMed: 23671105]
27. Zhang Z, et al. Chlorogenic Acid Ameliorates Experimental Colitis by Promoting Growth of Akkermansia in Mice. Nutrients 9(2017).
28. Furusawa Y, et al. Commensal microbe-derived butyrate induces the differentiation of colonic regulatory T cells. Nature 504, 446–450 (2013). [PubMed: 24226770]
29. Madsen KL, Doyle JS, Jewell LD, Tavernini MM & Fedorak RN Lactobacillus species prevents colitis in interleukin 10 gene-deficient mice. Gastroenterology 116, 1107–1114 (1999). [PubMed: 10220502]
30. Galdeano CM & Perdigon G The probiotic bacterium Lactobacillus casei induces activation of the gut mucosal immune system through innate immunity. Clin Vaccine Immunol 13, 219–226 (2006). [PubMed: 16467329]
31. Geier MS, Butler RN, Giffard PM & Howarth GS Lactobacillus fermentum BR11, a potential new probiotic, alleviates symptoms of colitis induced by dextran sulfate sodium (DSS) in rats. Int J Food Microbiol 114, 267–274 (2007). [PubMed: 17150273]
32. Sartor RB Therapeutic manipulation of the enteric microflora in inflammatory bowel diseases: antibiotics, probiotics, and prebiotics. Gastroenterology 126, 1620–1633 (2004). [PubMed: 15168372]
33. Guandalini S Use of Lactobacillus-GG in paediatric Crohn's disease. Dig Liver Dis 34 Suppl 2, S63–65 (2002). [PubMed: 12408443]
34. Zocco MA, et al. Efficacy of Lactobacillus GG in maintaining remission of ulcerative colitis. Aliment Pharmacol Ther 23, 1567–1574 (2006). [PubMed: 16696804]
35. Oliva S, et al. Randomised clinical trial: the effectiveness of Lactobacillus reuteri ATCC 55730 rectal enema in children with active distal ulcerative colitis. Aliment Pharmacol Ther 35, 327–334 (2012). [PubMed: 22150569]
36. Png CW, et al. Mucolytic bacteria with increased prevalence in IBD mucosa augment in vitro utilization of mucin by other bacteria. Am J Gastroenterol 105, 2420–2428 (2010). [PubMed: 20648002]
37. Fabia R, et al. Impairment of bacterial flora in human ulcerative colitis and experimental colitis in the rat. Digestion 54, 248–255 (1993). [PubMed: 8243838]
38. Rakoff-Nahoum S, Paglino J, Eslami-Varzaneh F, Edberg S & Medzhitov R Recognition of commensal microflora by toll-like receptors is required for intestinal homeostasis. Cell 118, 229–241 (2004). [PubMed: 15260992]
39. Lee Y, et al. Bilirubin Nanoparticles as a Nanomedicine for Anti-inflammation Therapy. Angew Chem Int Ed Engl 55, 7460–7463 (2016). [PubMed: 27144463]
40. Kim DE, et al. Bilirubin nanoparticles ameliorate allergic lung inflammation in a mouse model of asthma. Biomaterials 140, 37–44 (2017). [PubMed: 28624706]
41. Lee S, Lee Y, Kim H, Lee DY & Jon S Bilirubin Nanoparticle-Assisted Delivery of a Small Molecule-Drug Conjugate for Targeted Cancer Therapy. Biomacromolecules 19, 2270–2277 (2018). [PubMed: 29712433]
42. Cho I & Blaser MJ The human microbiome: at the interface of health and disease. Nat Rev Genet 13, 260–270 (2012). [PubMed: 22411464]
43. Lynch SV & Pedersen O The Human Intestinal Microbiome in Health and Disease. N Engl J Med 375, 2369–2379 (2016). [PubMed: 27974040]

44. Pietroiusti A, Magrini A & Campagnolo L New frontiers in nanotoxicology: Gut microbiota/microbiome-mediated effects of engineered nanomaterials. Toxicol Appl Pharmacol 299, 90–95 (2016). [PubMed: 26723910]
45. Javurek AB, et al. Gut Dysbiosis and Neurobehavioral Alterations in Rats Exposed to Silver Nanoparticles. Sci Rep 7, 2822 (2017). [PubMed: 28588204]
46. Qiu K, Durham PG & Anselmo AC Inorganic nanoparticles and the microbiome. Nano Research 11, 4936–4954 (2018).
47. Mosquera MJ, et al. Immunomodulatory nanogels overcome restricted immunity in a murine model of gut microbiome-mediated metabolic syndrome. Sci Adv 5, eaav9788 (2019). [PubMed: 30944865]
48. Lee Y, Lee S & Jon S Biotinylated Bilirubin Nanoparticles as a Tumor Microenvironment-Responsive Drug Delivery System for Targeted Cancer Therapy. Adv Sci (Weinh) 5, 1800017 (2018). [PubMed: 29938184]
49. Reissig JL, Storminger JL & Leloir LF A modified colorimetric method for the estimation of N-acetylamino sugars. J Biol Chem 217, 959–966 (1955). [PubMed: 13271455]
50. McCoy KD, Geuking MB & Ronchi F Gut Microbiome Standardization in Control and Experimental Mice. Curr Protoc Immunol 117, 23 21 21–23 21 13 (2017). [PubMed: 28369684]
51. Seekatz AM, et al. Fecal Microbiota Transplantation Eliminates Clostridium difficile in a Murine Model of Relapsing Disease. Infect Immun 83, 3838–3846 (2015). [PubMed: 26169276]
52. Schloss PD, et al. Introducing mothur: open-source, platform-independent, community-supported software for describing and comparing microbial communities. Appl Environ Microbiol 75, 7537–7541 (2009). [PubMed: 19801464]
53. Kozich JJ, Westcott SL, Baxter NT, Highlander SK & Schloss PD Development of a dual-index sequencing strategy and curation pipeline for analyzing amplicon sequence data on the MiSeq Illumina sequencing platform. Appl Environ Microbiol 79, 5112–5120 (2013). [PubMed: 23793624]

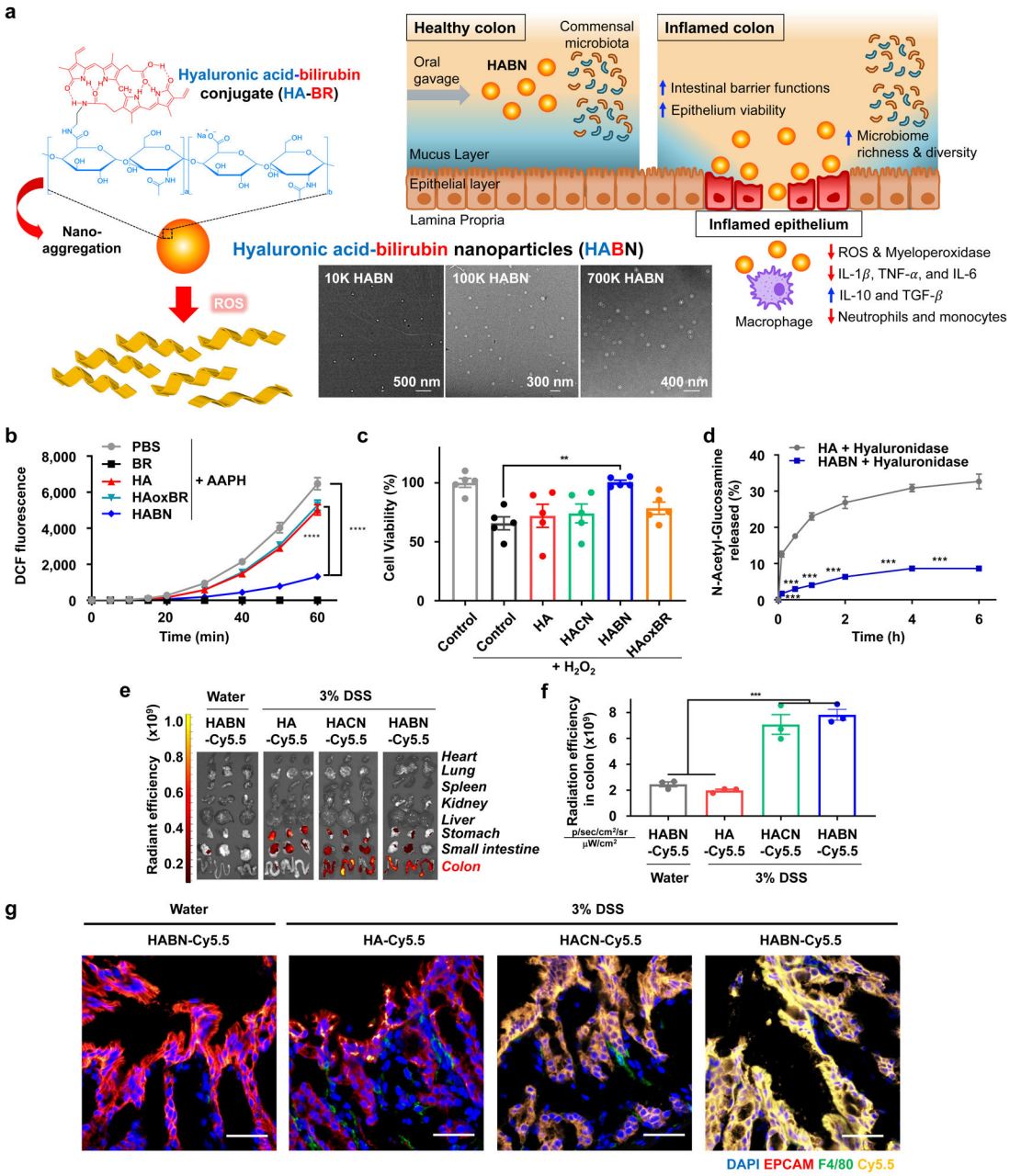

Figure 1. Hyaluronic acid-bilirubin nanomedicine (HABN) localizes in inflamed colon in DSS-treated mice.

a, Schematic of HABN self-assembled from hyaluronic acid-bilirubin conjugate (HA-BR) and their TEM images. HABN accumulates in inflamed colon and exerts therapeutic effects against acute colitis. Scale bars = 500 nm (10K HABN), 300 nm (100K HABN), and 400 nm (700K HABN). **b,** Fluorescence signals of DCF oxidized from DCFDA (50 μM) by peroxy radicals generated from 1 mM of AAPH at 37°C in the presence of BR (50 μM), HA (1 mg/ml), HABN (1 mg/ml), or PBS. **c**, Viability of HT-29 cells was measured with CCK-8 assay after overnight treatment with 500 μg/ml of HA, HACN, HABN, HAoxBR, or PBS in the presence of 100 μM H_2O_2. **d**, Generation of N-acetyl-glucosamine after treatment of 1

mg/ml HA, or HABN with 100 IU/ml hyaluronidase (HYAL)-II. **e-f**, After 6 h of treating animals with 7.5 mg/kg of HA-Cy5.5, HACN-Cy5.5, or HABN-Cy5.5, their organs were imaged by IVIS (**e**) and quantified for Cy5.5 fluorescence signal (**f**). **g,** Healthy or DSS-colitis mice were orally administered on day 6 with 7.5 mg/kg of HA-Cy5.5, HACN-Cy5.5, or HABN-Cy5.5 (equivalent mass of Cy5.5), and colon tissues were excised after 6 h, stained with anti-F4/80 and anti-EPCAM antibodies, and visualized by confocal microscopy. Scale bars = 40 μm. Shown are representative images from 6 slides with n = 3 animals from 2 independent experiments. Data are presented as mean ± s.e.m. from a representative experiment (n = 5 biologically independent samples for **b-d** and n = 3 biologically independent animals for **e-g**) from 2 independent experiments. *$p < 0.05$, **$p < 0.01$, ***$p < 0.001$, ****$p < 0.0001$, analyzed by one-way (**c,f**) or two-way (**b,d**) ANOVA with Tukey's HSD multiple comparison post hoc test.

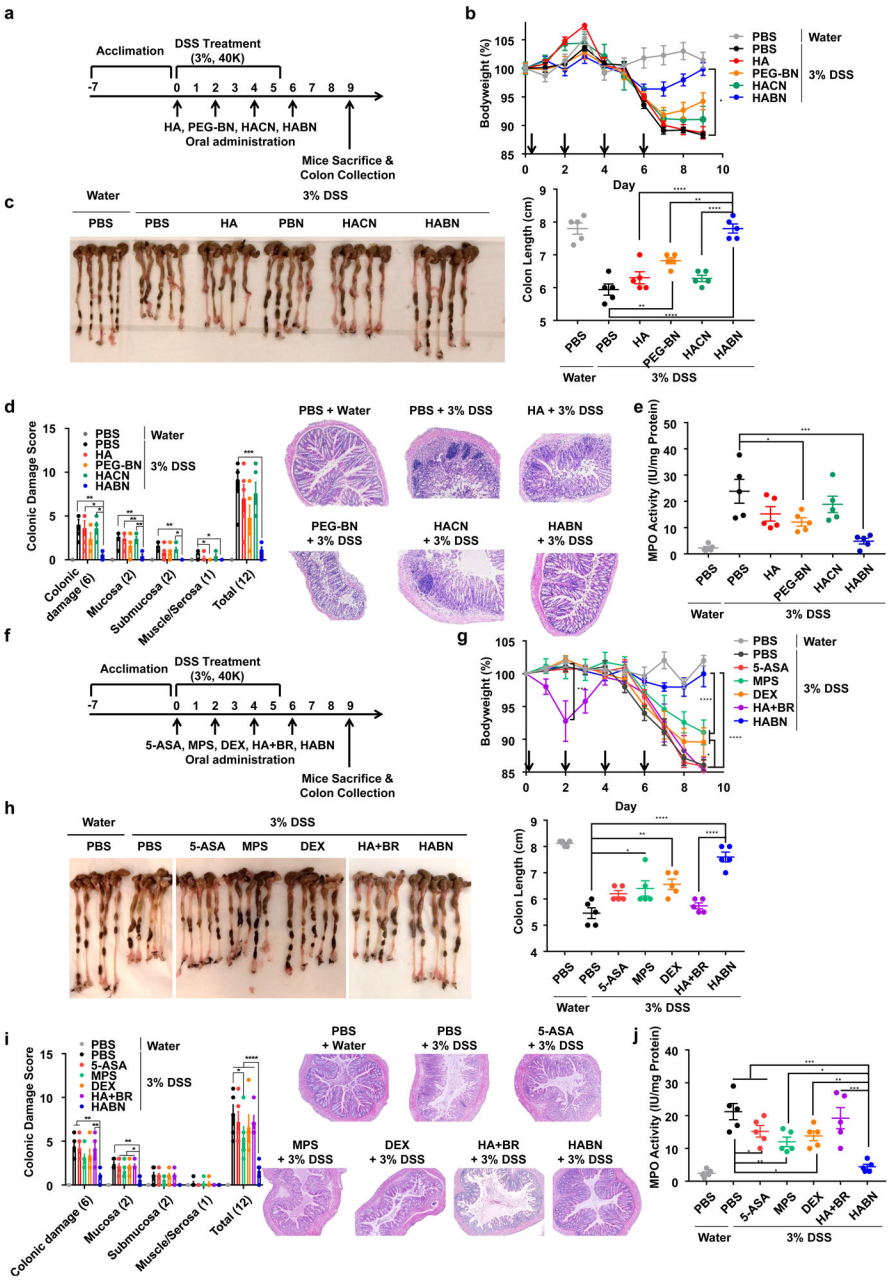

Figure 2. HABN exerts strong efficacy in a murine model of colitis.

a, C57BL/6 mice were provided with water or 3% DSS-containing water for 6 days. On days 0, 2, 4, and 6, mice were orally administered with PBS or 30 mg/kg of HA, HACN, HABN (with 100K HA at equivalent mass) or PEG-BN (equivalent mass of bilirubin as in HABN). **b,** Daily bodyweight changes in each group for 9 days. **c-e,** On day 9, animals were euthanized, and (**c**) colon length, (**d**) colonic damage scores, and (**e**) colonic MPO activity were measured. **f,** C57BL/6 mice were provided with water or 3% DSS-containing water for 6 days. On days 0, 2, 4, and 6, mice were orally administered with PBS or 5-ASA (30 mg/kg), MPS (1 mg/kg), DEX (1 mg/kg), HA+BR (equivalent mass of bilirubin and HA as in HABN), or HABN (with 100K HA at equivalent mass, 30 mg/kg). **g,** Daily bodyweight

changes in each group for 9 days. **h-j,** On day 9, animals were euthanized, and (**h**) colon length, (**i**) colonic damage scores, and (**j**) colonic MPO activity were measured. Data are presented as mean ± s.e.m. from a representative experiment (n = 5 biologically independent animals) from **(a-e)** 4 independent experiments or (**f-j**) 2 independent experiments. *$p <$ 0.05, **$p < 0.01$, ***$p < 0.001$, ****$p < 0.0001$, analyzed by (**c,d,e,h,i,j**) oneway or (**b,g**) two-way ANOVA with Tukey's HSD multiple comparison post hoc test.

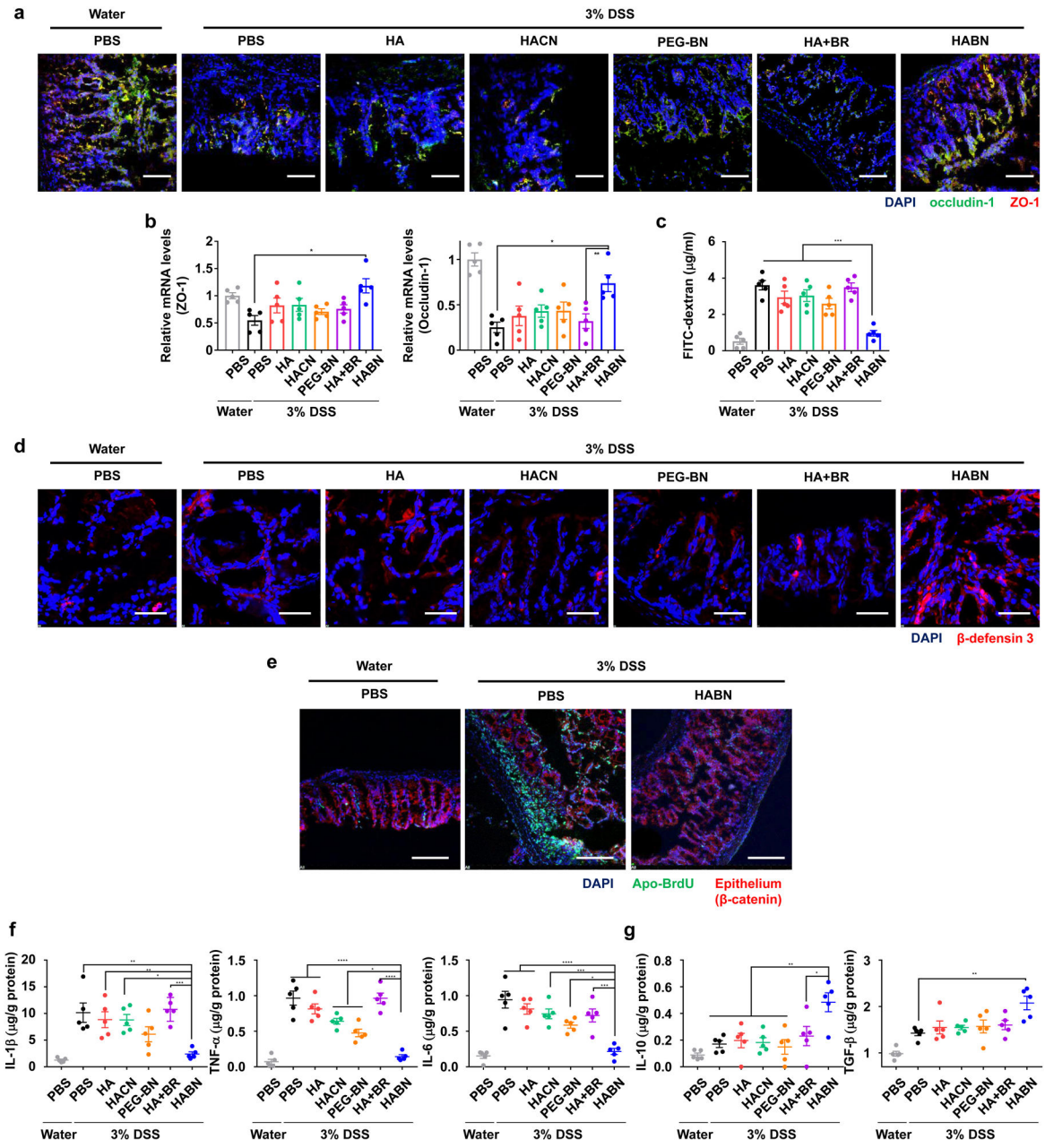

Figure 3. HABN protects colonic epithelium.

a,b, Healthy or DSS-colitis mice were orally administered on day 0, 2, 4, and 6 with PBS or 30 mg/kg of HA, HACN, PEG-BN, HA+BR, or HABN (equivalent mass of HA and bilirubin), and colon tissues were excised and analyzed for the (**a**) expression patterns and (**b**) mRNA levels of ZO-1 and occludin-1. **c**, Intestinal barrier functions were assessed in these mice by oral gavage of 4 MW FITC-dextran on day 9, followed by measuring the FITC-dextran signal in blood after 4 hr. **d,** Expression pattern of beta-defensin 3 was visualized by confocal microscopy. **e**, Colon tissues from healthy or DSS-colitis mice treated as shown were processed by the TUNEL assay, followed by visualization by confocal microscopy. Scale bars =100 μm (**a, d**). 50 μm (**e**). **f-g**, On day 9, colon tissues were

analyzed for the concentrations of (**f**) pro-inflammatory and (**g**) anti-inflammatory cytokines. Shown are representative images from 10 slides with n = 5 biologically independent animals from 2 independent experiments. Data are presented as mean ± s.e.m. *$p < 0.05$, **$p < 0.01$, ***$p < 0.001$, and ****$p < 0.0001$, analyzed by one-way ANOVA with Tukey's HSD multiple comparison post hoc test.

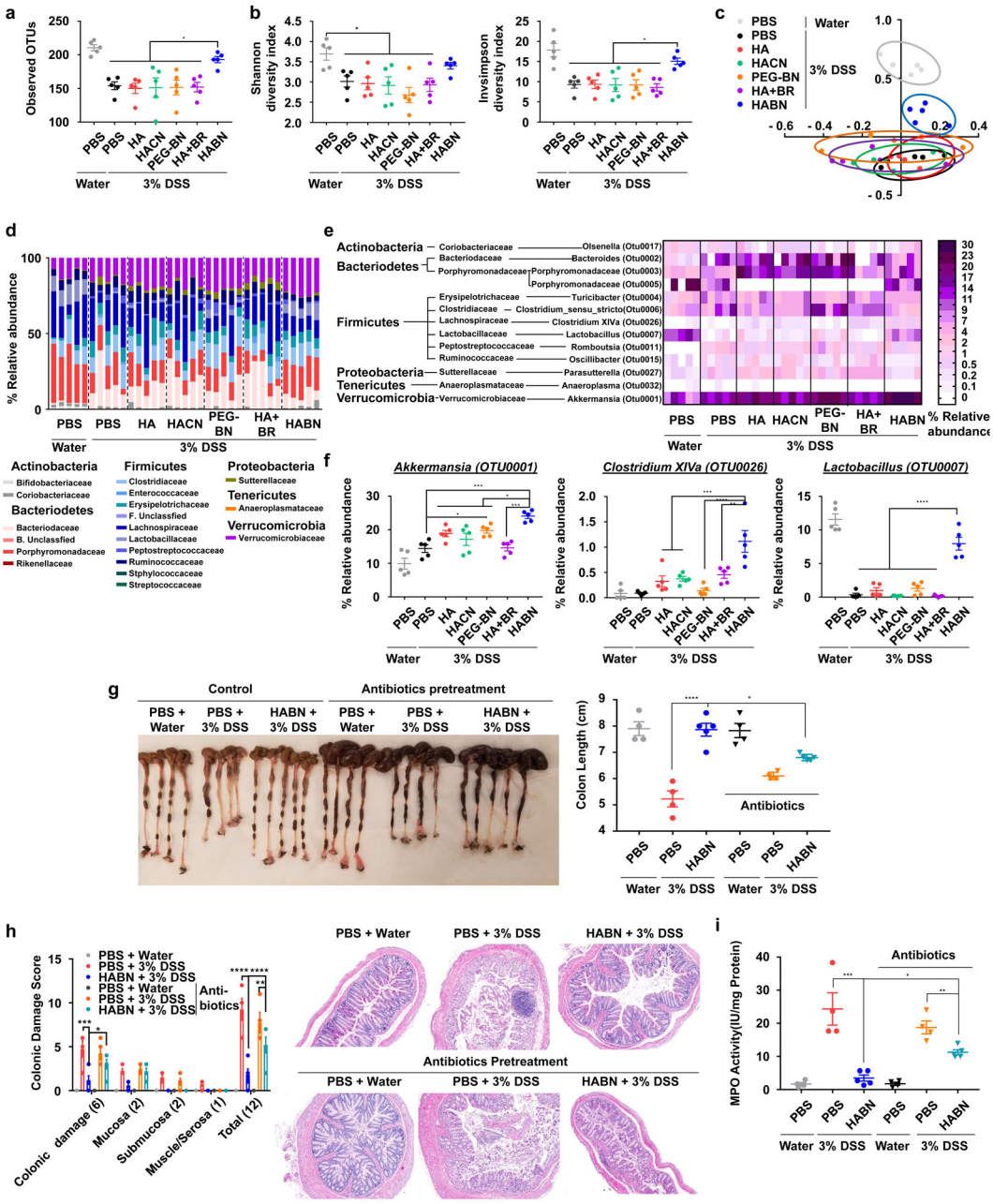

Figure 4. HABN alters the composition of gut microbiome.

a-f, C57BL/6 mice were provided with 3% DSS in drinking water for 6 days. Mice were treated as above in Figure 3. Feces collected on day 9 were analyzed for gut microbiome by 16S rRNA sequencing. **a**, Estimation of microbial community observed OTU (operational taxonomic unit) richness and **b,** α-diversity (Shannon and inverse Simpson indices). **c**, NMDS plot illustrating the gut microbiome β-diversity. Each point represents each mouse, based on a subsample of 1122 OTU. **d**, Relative abundance of gut microbiome. Phylum and family level taxonomy are presented as percentage of total sequences. **e**, Heatmap of the relative abundance of family-level taxa (rows) for each mouse (columns). The abundance is shown as relative percentage. **f**, Relative abundance of select taxa. **g-i,** C57BL/6 mice were

pretreated for 5 days with a cocktail of antibiotics (ampicillin, metronidazole, vancomycin, and neomycin) added to the drinking water and then provided with water or 3% DSS-containing water for 6 days. On days 0, 2, 4, and 6, mice were orally administered with PBS or 30 mg/kg of HABN. On day 9, animals were euthanized, and (**g**) colon length, (**h**) colonic damage scores, and (**i**) colonic MPO activity were measured. Data are presented as mean ± s.e.m. from a representative experiment (n = 4 biologically independent animals for PBS control groups in (**g-i**) and n = 5 biologically independent animals for all other panels) from (**a-f**) 4 and (**g-i**) 2 independent experiments. *$p < 0.05$, **$p < 0.01$, ***$p < 0.001$, ****$p < 0.0001$, analyzed by one-way ANOVA with Tukey's HSD multiple comparison post hoc test.

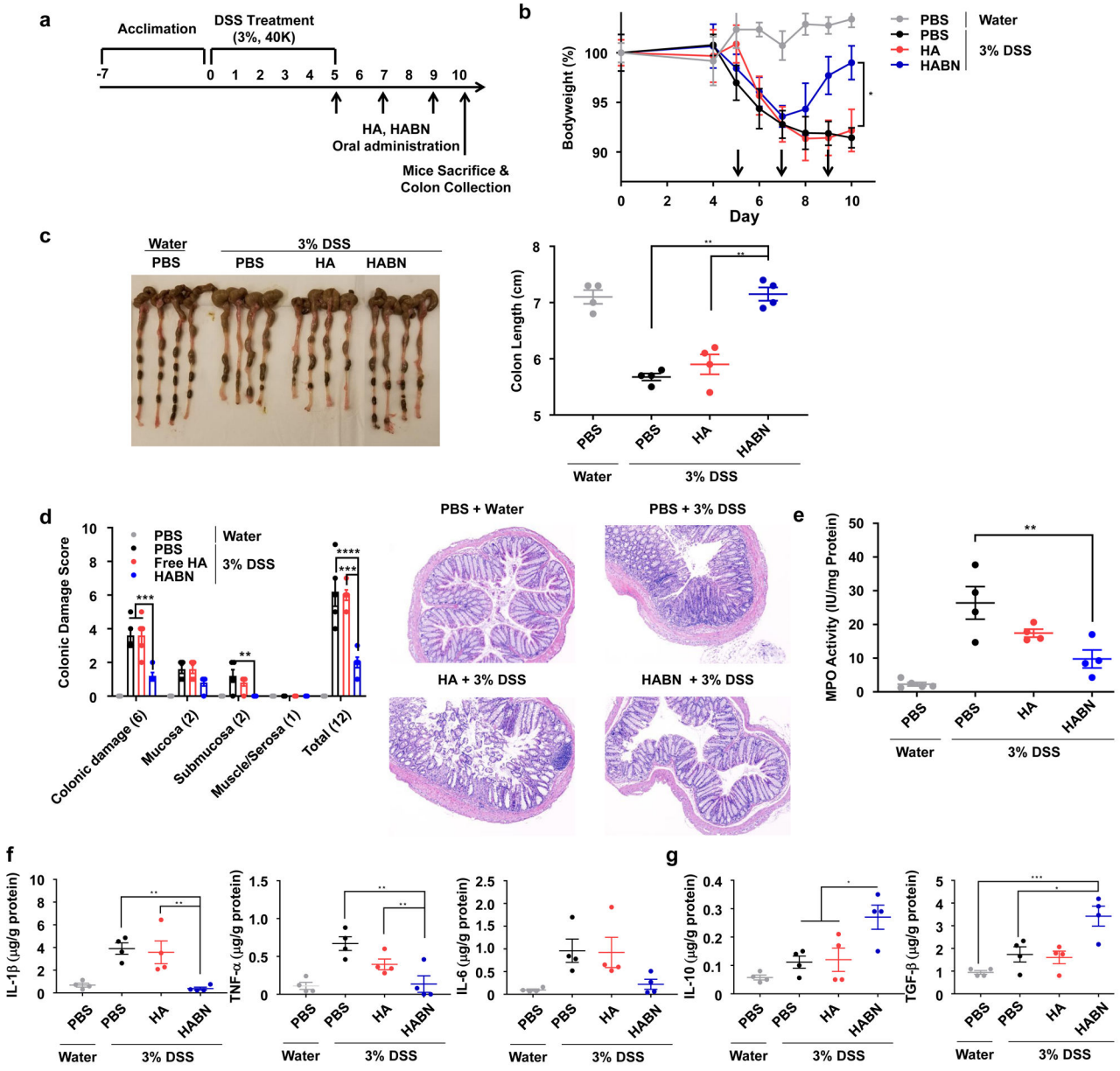

Figure 5. HABN alleviates colitis in a delayed therapeutic setting.

a-g, C57BL/6 mice were provided with water or 3% DSS-containing water for 5 days. On days 5, 7, and 9, mice were orally administered with PBS or 30 mg/kg of HA, HABN (with 100K HA at equivalent mass) **b,** Daily bodyweight changes in each group for 9 days. **c-g,** On day 9, animals were euthanized, and (**c**) colon length, (**d**) colonic damage scores, (**e**) colonic MPO activity, and local concentrations of (**f**) pro-inflammatory and (**g**) anti-inflammatory cytokines were quantitated. Data are presented as mean ± s.e.m. from a representative experiment (n = 4 biologically independent animals) from 4 independent experiments. *$p < 0.05$, **$p < 0.01$, ***$p < 0.001$ analyzed by (**c,e-g**) one-way or (**b,d**) two-way ANOVA with Tukey's HSD multiple comparison post hoc test.